Bulletin of the Chemical Society of Japan, 2025, **98**, uoaf076
https://doi.org/10.1093/bulcsj/uoaf076
Advance access publication 29 August 2025

Articles

Photoexcitation dynamics of azaphosphole compounds: effects of substituents and solvents

Rio Kitakado[1], Rika Takegami[2], Kaori Fujii[3], Hiroaki Nakagomi[4], Nina Murayama[4], Yoshihiro Matano[5], Haruyuki Nakano[6], Kanami Sugiyama[7], Masahiro Higashi[8], Yoshifumi Kimura[1,2,*]

[1]Deparment of Applied Chemistry, Graduate School of Science and Engineering, Doshisha University, 1-3 Tatara Miyakodani, Kyotanabe, Kyoto 610-0321, Japan

[2]Department of Molecular Chemistry and Biochemistry, Faculty of Science and Engineering, Doshisha University, 1-3 Tatara Miyakodani, Kyotanabe, Kyoto 610-0321, Japan

[3]Nanocarbon Material Research Institute, National Institute of Advanced Industrial Science and Technology, 1-1-1 Higashi, Tsukuba, Ibaraki 305-8565, Japan

[4]Department of Fundamental Sciences, Graduate School of Science and Technology, Niigata University, Ikarashi, Nishi-ku, Niigata 950-2181, Japan

[5]Department of Chemistry, Faculty of Science, Niigata University, Ikarashi, Nishi-ku, Niigata 950-2181, Japan

[6]Department of Chemistry, Graduate School of Science, Kyushu University, 744 Motooka, Nishi-ku, Fukuoka 819-0395, Japan

[7]Department of Molecular Engineering, Graduate School of Engineering, Kyoto University, Kyoto Daigaku-katsura, Nishikyo-ku, Kyoto 615-8510, Japan

[8]Department of Complex Systems Science, Graduate School of Informatics, Nagoya University, Furo-cho, Chikusa-ku, Nagoya 464-8601, Japan

*Corresponding author: Department of Applied Chemistry, Graduate School of Science and Engineering, Doshisha University, 1-3 Tatara Miyakodani, Kyotanabe, Kyoto 610-0321, Japan. Email: yokimura@mail.doshisha.ac.jp

Yoshifumi Kimura
Yoshifumi Kimura received his bachelor's degree from Kyoto University in 1987 and his PhD from Kyoto University in 1992. Successively, he became an assistant professor in Kyoto University. In 2001, he became an associate professor in Kyoto University. In 2012, he moved to Hosei University as a professor. A year later, he became a professor in Doshisha University.

Abstract

Photoexcitation dynamics of a series of 2-aryl-3H-1,3-benzazaphosphole oxides (ABPO) were studied using ultrafast time-resolved fluorescence spectroscopy and transient absorption spectroscopy. The fluorescence quantum yields and lifetimes strongly depended on the substituents on the phenyl ring at the 2-position, and generally fluorescence lifetimes were very short. Compound (**1d**) that has a 4-(*N,N*-diphenylamino)phenyl group at the 2-position showed intense fluorescence in nonpolar solvents, although the fluorescence was quite weak in polar solvents. The time-resolved fluorescence spectrum of **1d** showed a large dynamic shift, accompanied by a decrease in fluorescence intensity. The transient absorption spectrum of **1d** showed complex spectral dynamics. From the singular value decomposition analysis of the time-resolved spectra, the spectral dynamics were assigned to the charge transfer formation accompanying the rotation of the phenyl ring at 2-position predicted by the theoretical calculations (K. Sugiyama et al., *J. Phys. Chem. B*, 2025, *129,* 2701). A compound with an *ortho*-hydroxyphenyl at the 2-position (**1e-OH**) showed intramolecular proton transfer in aprotic solvents, showing dual fluorescence from the normal and tautomer bands. In methanol, a new fluorescence band appeared besides the bands from the normal and tautomer states, which was assigned to the hydrogen-bonding complex with the solvent by the theoretical calculations.

Keywords: azaphosphole, charge transfer, proton transfer.

[Received on 16 June 2025; revised on 5 August 2025; accepted on 7 August 2025; corrected and typeset on 29 August 2025]

Graphical Abstract

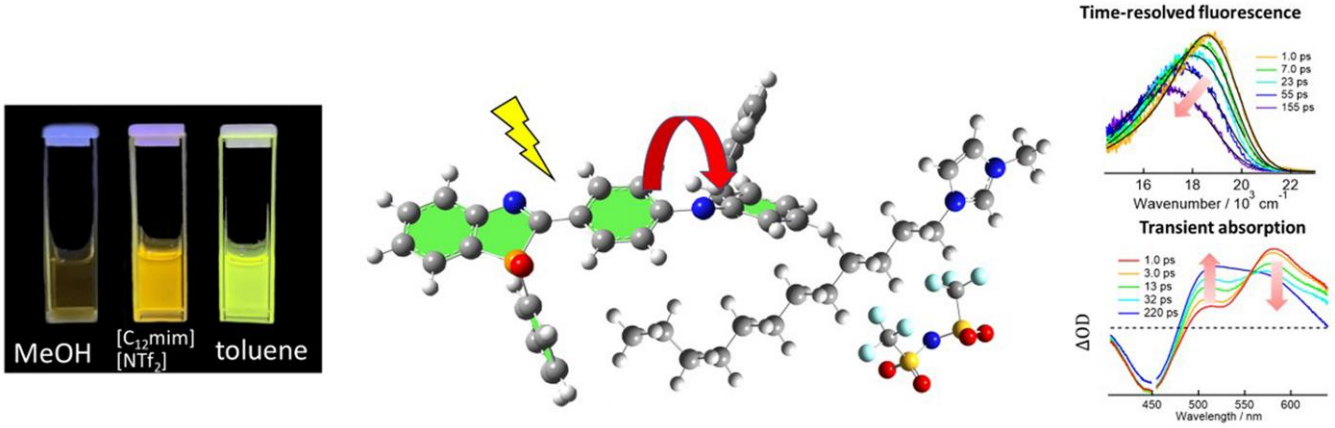

1. Introduction

Arene-fused phosphole derivatives are attractive compounds for photoelectrochemical applications, such as organic light-emitting diodes, fluorescence imaging, photochromic materials, organic solar cells, and so on.[1–12] Among these phosphole derivatives, 2-arylbenzo[*b*]phosphole oxides (**P1**, Fig. 1) have received significant attention because their photochemical properties can be easily controlled by changing the substituents on the phenyl ring at the 2-position (-R in Fig. 1). Notably, many **P1** derivatives are highly fluorescent with large fluorescence quantum yields due to the rigid P-bridged stilbene-like skeleton, and their emission wavelengths are sensitive to the substituents of the 2-aryl group.[13,14] To dramatically change the emissive properties of **P1** without the assistance of peripheral substituents, replacement of the β-methine unit of the phosphole ring with a nitrogen atom is a promising approach. Recently, we successfully synthesized a new class of phosphole derivatives, 2-aryl-3H-1,3-benzazaphosphole oxides (ABPO), by replacing the β-methine unit of the phosphole ring with a nitrogen atom.[15] We synthesized a series of ABPO by introducing various substituents at the phenyl group attached to the 2-position (see Fig. 1) and evaluated their fundamental optical properties. It has been revealed that most of the ABPO are less fluorescent and have much lower fluorescence quantum yields than their phosphole counterparts **P1**. One exception was a compound with a 4-(*N*,*N*-diphenylamino)phenyl group at the 2-position (**1d**). In contrast to the other ABPO, **1d** showed intense fluorescence in nonpolar solvents. However, upon increasing the polarity of solvents, the fluorescence spectra of **1d** showed a large red shift with a decrease in the quantum yield. Very recently, Sugiyama et al.[16] performed detailed electronic state calculations on this compound by explicitly considering the solvent effect. They applied the quntaum chemical and molecular mechanical (QM/MM) calculation to the electronic excited state of **1d** in various solvents and succeeded in reproducing the solvent effect on the Stokes shift. Their calculations suggested that the electronic excited state had a charge transfer (CT) character, showing twisting of the phenyl ring at the 2-position. The calculation suggested the existence of a twisted intramolecular CT (TICT) state upon further rotation of the phenyl ring, which may be the reason for the low emission in polar solvents. However, the details of this process remain unclear. Clarification of the excited-state dynamics of **1d** is one of the aims of this study.

In our previous study,[15] we demonstrated that a compound with a 2-hydroxyphenyl group at the 2-position (**1e-OH**) showed dual fluorescence owing to the excited-state intramolecular proton transfer (ESIPT) reaction, as observed for compounds with similar structures.[17–25] The photoexcited phenol–imine (OH) tautomer transfers a hydroxy proton to

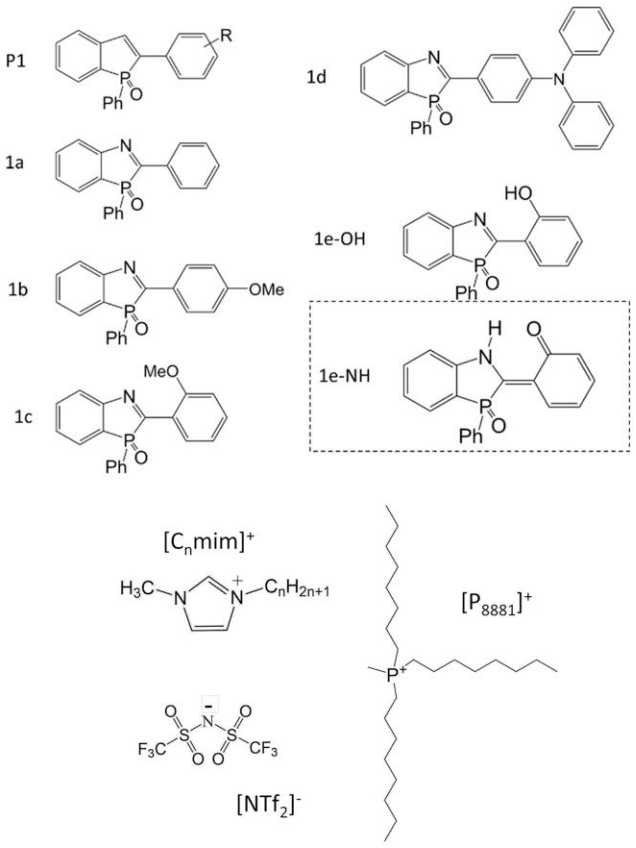

Fig. 1. Chemical structures of the molecules and ions used in this study. R denotes various substituents. **1e-NH** is a tautomeric form of **1e-OH**, which is unstable in the electronic ground state.

the nitrogen atom to generate a more thermally stable keto–NH (NH) tautomer in the excited state. The NH tautomer (**1e-NH**) undergoes relaxation via radiative and nonradiative pathways to the ground state, followed by tautomerization to the more stable OH form. It has been demonstrated that ESIPT occurs very rapidly (<0.2 ps) and that the decay of the keto-tautomer is also fast in toluene and dichloromethane (DCM).[15] The very fast ESIPT is consistent with previously observed kinetics.[18,20] However, a detailed investigation of the solvent effect, especially in protic solvents, has not yet been conducted.

In the present paper, we report the effects of substituents and solvents on the photoexcitation dynamics of ABPO compounds using time-resolved fluorescence and transient absorption measurements. We mainly focused on the following 2 points. One is the clarification of the solvent effect on **1d**. By measuring the time-resolved fluorescence spectra, we investigated how the fluorescence dynamics of **1d** differed from those of **1a**, **1b**, and **1c**. As solvents for **1d**, we used 6 conventional organic solvents, including a protic solvent, from nonpolar to polar solvents. Ionic liquids (ILs) have also been used as solvents. ILs are unique polar solvents, whose properties can be controlled by the choice of cations and anions.[26] In this study, we used 2 imidazolium-based ILs with different alkyl chain lengths (1-methyl-3-butylimidazoium $[C_4mim]^+$ and 1-methyl-3-dodecylimidazolium $[C_{12}mim]^+$) and one phosphonium-based ionic liquid (trioctylmethylphosphonium $[P_{8881}]^+$) with the same anion (bis(trifluoromethylsulfonyl)amide $[NTf_2]^-$) (see Fig. 1). $[C_4mim][NTf_2]$ is a typical hydrophobic IL, the properties of which have been well studied.[26,27] Although the dielectric constant of $[C_4mim][NTf_2]$ was not very high,[28] the polarity estimated by the solvatochromic parameter was as high as that of acetonitrile (ACN).[29] Two other ILs have long alkyl chains, and the long alkyl chain brings about a nonpolar domain in ILs. Although these ILs show relatively large polarity similar to that of $[C_4mim][NTf_2]$,[30] they exhibit a heterogeneous structure owing to the segregation between the polar and nonpolar parts,[31–34] which results in unique solvent effects.[35–39] It is interesting to note how structural heterogeneity appeared in the CT dynamics of **1d**. Comparison among these 3 ILs will clarify the role of the nonpolar domain in ILs on the reaction of **1d**. To test the plausible existence of the TICT state, transient absorption spectroscopy was performed. The excited-state dynamics are discussed in detail based on the spectroscopic data and theoretical calculations. The other is the solvent effect on the ESIPT of **1e-OH**. In the previous paper, we presented time-resolved fluorescence data of **1e-OH** in toluene and DCM.[15] In this study, we extended the solvent to aprotic and protic polar solvents. We found that the excited-state dynamics in methanol (MeOH) are quite different from those in other aprotic solvents. The reaction mechanism is discussed in detail based on spectroscopic data and density functional theory (DFT) calculations.

2. Experimental

2.1 Materials

Compounds **1a**, **1b**, **1c**, **1d**, and **1e-OH** were synthesized according to literature.[15] Spectroscopic-grade solvents (toluene, tetrahydrofuran [THF], DCM, acetone, ACN, and MeOH) were purchased from Nacalai Tesque and Wako Chemicals and used without further purification. $[C_4mim][NTf_2]$, $[C_{12}mim][NTf_2]$, and $[P_{8881}][NTf_2]$ were synthesized according to literature[30] and dried before use under vacuum.

2.2 Spectroscopic measurements

The experimental setups for transient absorption and time-resolved fluorescence measurements are described in detail elsewhere.[40,41] For the transient absorption measurements, the optical density of the sample solution was adjusted to be ~0.6 at the excitation wavelength, using an optical cell with a 1-mm path length. For the fluorescence measurements using the optical Kerr gate, the optical density of the sample solution was ~1.0 at the excitation wavelength, using an optical cell with a 1-mm path length. Most experiments were performed at an excitation wavelength of 400 nm; however, in some experiments, an excitation wavelength of 360 nm (or 350 nm) was chosen. Measurements were performed under the sample flow condition. The absorption spectrum of the sample solution was measured before and after the experiments, and in most cases, sample degradation by light was negligible. Absorption spectra were measured using UV-1800 or UV-2600 (Shimadzu), and the fluorescence spectra were measured using FP-6500 or EP-8300 spectrometers (JASCO). The absolute fluorescence quantum yields were measured using a Hamamatsu Photonics Quantaurus-QY spectrometer.

2.3 DFT calculations

The geometries were optimized using DFT for the S_0 state and time-dependent DFT (TD-DFT) for the S_1 state. The basis set used for the optimization was 6-311G(d,p).[42] The functional of DFT and TD-DFT was ωB97X-D.[43] The solvent effects were incorporated in both DFT and TD-DFT calculations using the polarizable continuum model (PCM) with the integral equation formalism variant.[44] The optimized geometries were confirmed to be minima by vibrational analysis. All the calculations were performed using the Gaussian 16 suite of programs.[45]

3. Results and discussion

3.1 Steady sate absorption and fluorescence spectra of 1a–1d

Figure 2a shows the steady-state absorption and fluorescence spectra of **1a–1d** in DCM. The addition of an electron-donating group to the phenyl ring resulted in a red shift of the absorption spectrum, as mentioned previously,[15] although the absorption and fluorescence spectra of **1a, 1b,** and **1c** did not show significant solvent effects (Supplementary Table S1). The absorption and fluorescence peaks of **1d** were significantly red-shifted to others. Although the fluorescence spectra of **1a–1c** did not show significant shift with solvent, the fluorescence spectrum of **1d** showed a large Stokes shift, especially in polar solvents, as shown in Fig. 2b,[15] and the fluorescence quantum yield was strongly dependent on the solvent polarity. In a solvent with a large Stokes shift, the fluorescence quantum yield decreased and the fluorescence lifetime became short. These values are listed in Supplementary Tables S1 and S2.

Supplementary Fig. S1 shows the plot of Stokes shift of **1d** against polarity scale based on the dielectric continuum model $F(\varepsilon_0, n)$ as:[46–48]

$$F(\varepsilon_0, n) = \frac{\varepsilon_0 - 1}{\varepsilon_0 + 2} - \frac{n^2 - 1}{n^2 + 2} \quad (1)$$

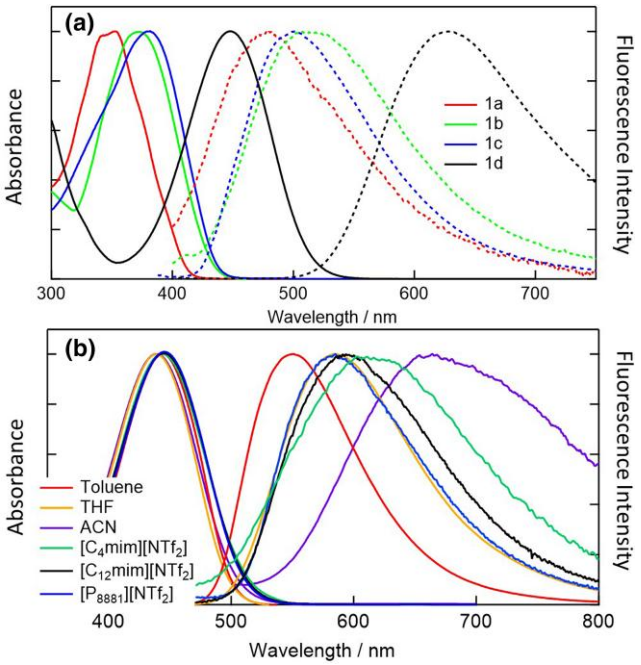

Fig. 2. a) Absorption and fluorescence spectra of **1a**, **1b**, **1c**, and **1d** in DCM. b) Absorption and fluorescence spectra of **1d** in various solvents. All spectra are normalized at the peak intensity.

where ε_0 is the static dielectric constant and n the optical refractive index of solvent. These parameters are listed in Supplementary Table S2. As shown, there holds a linear relationship between the polarity scale and the Stokes shift, suggesting that the CT character contributed to the electronic exited state.

3.2 Time-resolved spectroscopy of 1a–1c

Figure 3 shows the time-resolved fluorescence spectra of **1a** in DCM. The fluorescence showed an initial red shift, probably due to the solvation dynamics in the excited state within a few picoseconds. Subsequently, the intensity of the fluorescence appeared to decay monotonically. To estimate the decay constant of the fluorescence, we assumed that the fluorescence band is expressed by a single log normal function as:

$$I_i(t, \nu) = \begin{cases} h_i(t) \exp\left(-\ln 2 \left\{ \dfrac{\ln(1+\alpha_i(t))}{\gamma_i(t)} \right\}^2 \right) & \alpha > -1 \\ 0 & \alpha < -1 \end{cases} \quad (2)$$

where $\alpha_i(t) = 2\gamma_i(t)(\nu - \nu_i(t))/\Delta_i(t)$, h_i the peak height, ν_i the peak position, γ_i the asymmetric parameter, and Δ_i the bandwidth parameter, respectively. Here, subscript index i indicates the numbering of the spectral components. Here, only one spectral species is assumed, while later several spectral species are assumed for other systems. The details of the spectra fit are described in Supplementary Section S1. The black curves in Fig. 3 are the results of the fitting, which capture the spectral features well. The time profiles of the fluorescence peak position and fluorescence intensity estimated from the band integration are shown in Supplementary Fig. S2. The fluorescence intensity decayed monotonically as shown in Supplementary Fig. S2a and was well fitted by a single exponential function (decay constant τ_f). As shown in Supplementary Fig. S2b, the peak position showed an initial

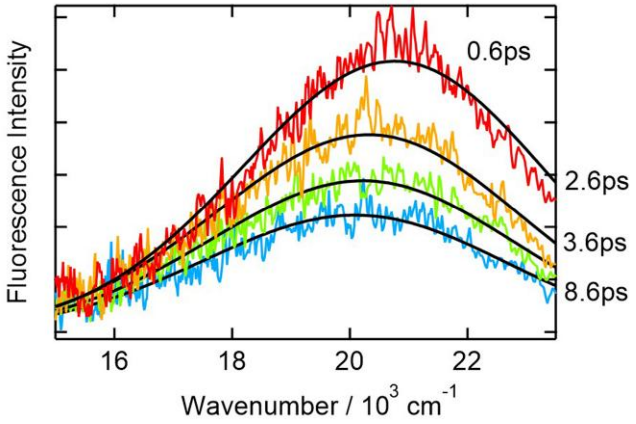

Fig. 3. Time-resolved fluorescence spectra of **1a** in DCM.

shift with time. The extent of the initial peak shift was ca. 500 cm^{-1}, and the shift was fit by a single exponential function as:

$$\nu_P(t) = \nu_\infty + \Delta\nu \exp\left(-\frac{t}{\tau^P}\right) \quad (3)$$

The parameters obtained by the fit are listed in Supplementary Table S1. As represented by the small dynamic Stokes shift, the Stokes shift of **1a** is considered mostly from the intramolecular reorganization energy. The DFT and TD-DFT calculation results supported this idea. In Supplementary Table S3, we listed the electronic state energies and dipole moments of **1a** for the optimized geometries of S_0 and S_1 in toluene and ACN (PCM model), respectively. The oscillator strength of the transition from S_0 to S_1 for the optimized structure of the ground state was found to be quite small (0.005 in toluene and 0.008 in ACN), and the absorption from S_0 to S_2 is dominant (0.475 in toluene and 0.436 in ACN). The change of the dipole moment due to the transition is small, and the reorganization energy (difference of the energy of the same electronic state between different optimized geometries) mostly comes from the structure change as shown in Supplementary Fig. S3 (the Cartesian coordinates are summarized in Supplementary Table S4). In the ground state, the azaphosphole ring and the phenyl ring attached to the 2-position are almost planar, while in the electronic excited state, they are not planar. This kind of conformational change is the reason for the Stokes shift.

Upon addition of the electron-donating group at the *para* (**1b**) or *ortho* (**1c**) position, the fluorescence spectra showed a slight red shift, and the decay rate became slow (see Supplementary Fig. S4). The fluorescence decay rates of **1a**, **1b**, and **1c** in various solvents are summarized in Supplementary Table S1. The decay rates of **1a** were very short (e.g. 5.2 ps in toluene) and almost independent of the solvent, except for methanol (9.8 ps). The lifetime increased with the addition of an electron-donating group. This may be due to the stabilization of the excited state by introducing the electron-donating group. In order to check the possibility of the reaction path to a nonfluorescent state (e.g. a triplet state), the transient absorption spectra of **1a** in DCM were measured (Supplementary Fig. S5). Transient absorption bands from the excited state appeared at 420 and 570 nm, and both decayed with a similar time constant. Supplementary Fig. S5b shows

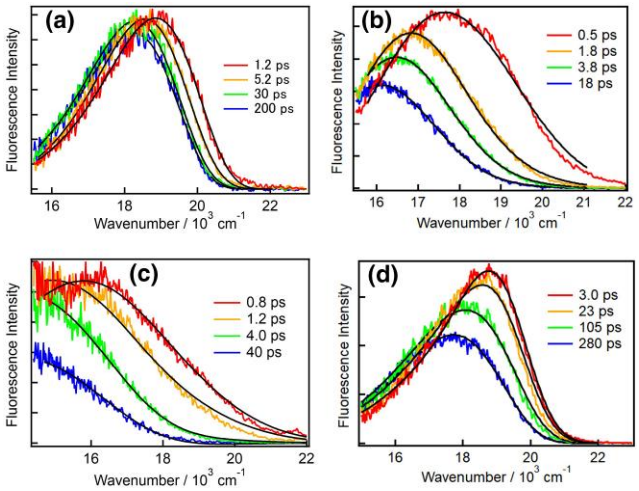

Fig. 4. Time-resolved fluorescence spectra of **1d** in a) toluene, b) DCM, c) ACN, and d) $[P_{8881}][NTf_2]$.

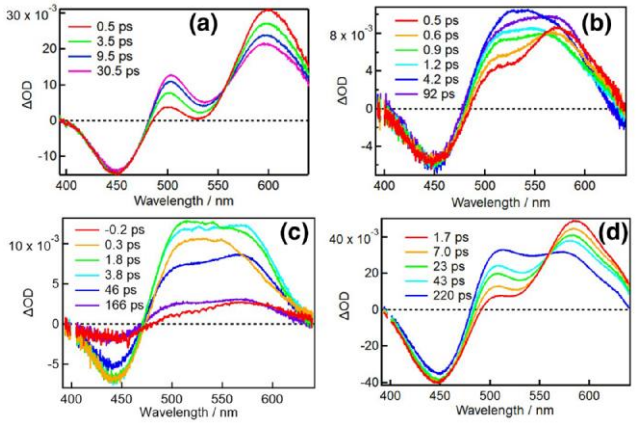

Fig. 5. Transient absorption spectra of **1d** in a) toluene, b) DCM, c) ACN, and d) $[P_{8881}][NTf_2]$.

a decay at 570 nm, and the decay was simulated by a single exponential function with a similar time constant (7.6 ps) to the fluorescence decay. We are not sure of the reason for the 10% difference between the fluorescence decay and transient absorption decay. No appearance of another absorption band after the decay of the excited state band may suggest the excited state decayed to the ground state. To assure this, we tried to measure the ground-state bleach recovery. However, the white continuum was too weak around 360 nm, and we could not confirm the recovery to the ground state.

3.3 Time-resolved spectroscopy of 1d

Figure 4a shows the time-resolved fluorescence of **1d** in toluene. The fluorescence peak position showed a small shift with time immediately after photoexcitation. Similar spectral dynamics were observed for the weakly polar and polar solvents (DCM and ACN), as shown in Fig. 4b and c, although the extent of the peak shift was much larger, and the intensity of the fluorescence decayed in accordance with the peak shift. The time-resolved fluorescence spectra in $[P_{8881}][NTf_2]$ is shown in Fig. 4d. The peak shift dynamics were slower than those of the other solvents. The results for the other solvents are shown in Supplementary Fig. S6. Although the time scales and extent of the shift were dependent on the solvent species, the dynamics were quite similar to one another.

The apparent fluorescence peak shifts are commonly observed in the solvation dynamics of dye molecules.[49,50] However, the initial large intensity decay with peak shift is not so common. To study the excited-state dynamics in more detail, we applied transient absorption measurements for the same system. Figure 5 shows the transient absorption spectra in the selected solvents. The apparent spectral features of the transient absorption in toluene were quite different from those of the fluorescence dynamics in toluene. Immediately after excitation, the absorption peak appeared at ~600 nm, which decreased with time. In contrast, the absorption at ~500 nm gradually increased. Because the wavelength of the spectral minimum around 540 nm corresponds to the peak wavelength of the fluorescence, it is probable that the spectral shift of the induced emission, which contributes to the transient absorption as a negative signal, causes an apparent spectral intensity change in the transient absorption. To test this possibility, we compared the transient absorption and time-resolved fluorescence spectra at the same delay time, as shown in Supplementary Fig. S7a and b. In the figure, the time-resolved fluorescence spectra are plotted downward (negative contribution as the induced emission). As shown in the figure, the peak of the fluorescence is at the same position as the minimum of the absorption spectra, suggesting that the induced emission contributes to the transient absorption spectrum. However, comparing the spectra at 5 and 25 ps, the intensity increase around 20,000 cm^{-1} (500 nm) is more apparent than the change in the fluorescence spectrum. Therefore, it is reasonable to consider that a new species with an absorption at ~500 nm appears with time.

Figure 5b shows the transient absorption spectra of **1d** in DCM. The spectral dynamics were quite different from those in toluene. The spectrum immediately after excitation is similar to that of toluene. However, within a picosecond, the absorbance at ~500 nm increased, and then the absorbance at ~600 nm increased. Similar spectral dynamics were obtained for the ACN solution (Fig. 5c). Supplementary Fig. S7c and d compares the transient absorption and time-resolved fluorescence at the same delay time in DCM. In contrast to the case of toluene, the negative peak position of the fluorescence red-shifted to the plateau of the transient absorption at ~18,500 cm^{-1}. With time, the fluorescence peak showed a more red shift, which may scrape the red region of the transient absorption. The transient absorption spectra in $[P_{8881}][NTf_2]$ were similar to those in toluene, as observed in the case of fluorescence (Fig. 4d). The spectral dynamics were very slow as fluorescence dynamics. The results for the other solvents are summarized in Supplementary Fig. S8.

3.4 Excited state reaction model of 1d and analysis based on singular value decomposition

According to theoretical calculations,[16] upon excitation, the Franck–Condon (FC) state of **1d** is a partially charge-transferred state, and the dipole moment of the FC state is larger than that of the ground state. By rotating the phenyl ring with $-N(ph)_2$, a more stable CT state is produced, which shows a larger dipole moment. Therefore, a large

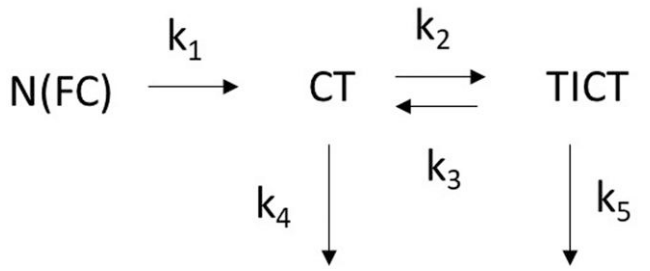

Scheme 1. Model reaction scheme of **1d**.

structural change was accompanied by the production of the CT state in the excited state. Theoretical calculations suggest that further rotation of the phenyl ring produces a more stable TICT state in polar solvents. In nonpolar solvents such as toluene, the TICT state has an energy similar to that of the CT state, but the energy of the TICT state decreases in polar solvents such as ACN. According to theoretical calculations, the oscillator strength from the TICT state to the ground state is nearly zero; therefore, the TICT state is dark in fluorescence.

Considering the above theoretical predictions,[16] we assume a typical reaction scheme in the TICT formation as shown in Scheme 1.[51]

In this scheme, we assume 3 electronic excited states: N (FC state), CT, and TICT. The rate constants k_4 and k_5 represent the sum of the nonradiative and radiative decay rates (nonreactive decay rate) from each state. We neglected the backward reactions from CT to N and assumed that the nonreactive decay of N is much slower than the rate to the CT state (k_1). The general solutions of these equations are given in Supplementary Section S2 under the initial concentrations of $[\mathrm{N}](t=0)=[\mathrm{N}]_0$, $[\mathrm{CT}]\ (t=0)=0$, and $[\mathrm{TICT}](t=0)=0$.[51]

Here, we consider the following special cases:

Case 1. Nonpolar solvent. No TICT formation. When $k_2 = 0$, the time profile of [CT] is given by a simple cascade reaction scheme as:

$$[\mathrm{CT}] = k_1[\mathrm{N}]_0\left\{\frac{1}{k_1-k_4}\exp(-k_4t) - \frac{1}{k_1-k_4}\exp(-k_1t)\right\} \quad (4)$$

In this case, the decay of the [CT] spectrum is determined by the sum of the radiative and nonradiative decays of the CT state.

Case 2. Polar solvent. The formation of the TICT rate k_2 and the nonreactive decay of TICT k_5 are much faster than the backward reaction from the TICT state, that is, k_2, k_4, $k_5 >> k_3$.

$$[\mathrm{CT}] = k_1[\mathrm{N}]_0\left\{\frac{1}{k_1-k_\mathrm{B}}\exp(-k_\mathrm{B}t) - \frac{1}{k_1-k_\mathrm{B}}\exp(-k_1t)\right\} \quad (5)$$

$$[\mathrm{TICT}] = k_1k_2[\mathrm{N}]_0\left\{\frac{1}{(k_1-k_5)(k_\mathrm{B}-k_5)}\exp(-k_5t) - \frac{1}{(k_1-k_\mathrm{B})(k_B-k_5)}\exp(-k_\mathrm{B}t) + \frac{1}{(k_1-k_5)(k_1-k_\mathrm{B})}\exp(-k_1t)\right\} \quad (6)$$

where

$$k_\mathrm{B} = k_2 + k_4$$

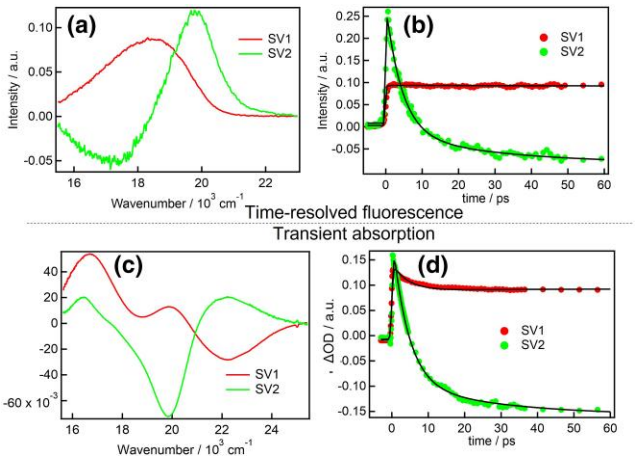

Fig. 6. SVD analysis of the time-resolved fluorescence spectra a) and b) and transient absorption spectra c) and d) of **1d** in toluene. The spectral component and the time profile of the first largest SV are denoted by SV1, and those of the 2nd largest ones are by SV2.

In reality, the spectral shift owing to solvation dynamics may contribute to the spectral dynamics, which makes an additional contribution to the spectrum.

Based on the above reaction scheme, we consider the time constants obtained by analyzing the time-resolved fluorescence and transient absorption spectra. In nonpolar solvents such as toluene, the energy level of TICT is nearly equal to that of CT according to theoretical calculations[16]; therefore, the 1st case is applicable considering the plausible activation barrier between the 2 states. The observed spectral dynamics corresponds to the reaction process from N to CT in the electronically excited state. From the similarity of apparent spectral dynamics, we classified toluene, THF, $[\mathrm{C_{12}min}][\mathrm{NTf_2}]$, and $[\mathrm{P_{8881}}][\mathrm{NTf_2}]$ into this group. On the other hand, the spectral dynamics in other solvents (DCM, acetone, ACN, MeOH, and $[\mathrm{C_4min}][\mathrm{NTf_2}]$) are quite different. Therefore, we assume that the TICT formation occurs in this group.

Although the apparent behavior of the time-resolved fluorescence and transient absorption spectra are different from each other, they should capture the same dynamics at different aspects. To obtain the unified time scales for both dynamics, we performed singular value decompositions (SVDs) for both spectra. At first, we discuss Case 1 where no TICT formation occurs. Figure 6a shows the spectral components of the 1st and 2nd largest singular values (SVs) of the time-resolved fluorescence spectra in toluene, and Fig. 6b shows their time profiles. We neglected the SV components more than the 2nd, because the SV of the 3rd component was much smaller than the 2nd SV (see Supplementary Table S5). The 1st spectral component shows a single broadband spectrum around 18,000 $\mathrm{cm^{-1}}$, and the 2nd component shows a negative value at a lower wavenumber and a positive value at a higher wavenumber. The intensity of the 1st component shows a fast decay and is almost constant. The spectral shift of the fluorescence was realized by the variation of the 2nd component from positive to negative. The spectral components of the transient absorption (Fig. 6c) are more complicated. The 1st component is similar to the averaged spectrum of transient absorption spectra shown in Fig. 5a, and the 2nd component is negative around 20,000 $\mathrm{cm^{-1}}$ (500 nm) and positive around 22,000 and 16,600 $\mathrm{cm^{-1}}$ (450 and 600 nm). By varying the 2nd

Table 1. Summary of the rate constants for the CT formation determined by the fluorescence data (FL) and by the transient absorption data (TA), and the rate of the TICT formation of **1d**, together with the value of the solvent viscosity.

Solvent	η/mPa s	k_{CT}/ps^{-1} FL	k_{CT}/ps^{-1} TA	k_{TICT}/ns^{-1}
Toluene	0.56[a]	0.098	0.088	–
THF	0.51[b]	0.53	0.77	–
DCM	0.44[c]	0.33	–	0.19
Acetone	0.31[a]	0.42		1.5
ACN	0.35[a]	0.27	–	7.7
MeOH	0.53[a]	0.29		48
[C_4mim][NTf_2]	55[d]	0.024	–	3.4
[C_{12}mim][NTf_2]	174[d]	0.020	0.023	–
[P_{8881}][NTf_2]	664[e]	0.015	0.015	–

[a]At 23 °C.[54]
[b]At 20 °C.[55]
[c]At 20 °C.[52]
[d]At 23 °C.[53]
[e]At 23 °C.[56]

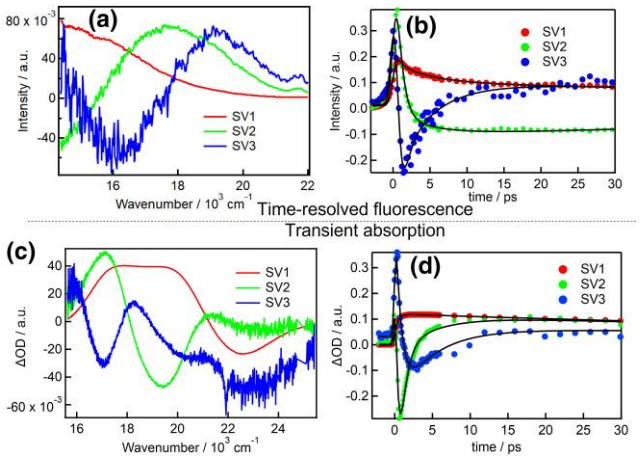

Fig. 7. SVD analysis of the time-resolved fluorescence spectra a) and b) and transient absorption spectra c) and d) of **1d** in ACN. The spectral component and the time profile of the first largest SV are denoted by SV1, and those of the 2nd and 3rd largest ones are by SV2 and SV3, respectively.

component from positive to negative with time, spectral intensity changes at 20,000 and 16,600 cm^{-1} were realized (Fig. 6d). We simultaneously fitted the time profiles of the SVD decompositions of both time-resolved fluorescence and transient absorption spectra using multiexponential functions with the same time constants as:

$$I(t) = \int dt' \sum_{i=1}^{n} a_i e^{-t/\tau_i} I_{rf}(t - t') \quad (7)$$

Here, $I_{rf}(t)$ is a system response function. In the fitting, the longest time constant was fixed as the fluorescence lifetime. The black curves in the figure show the fitting results that capture the trances well. The results in other solvents for Case 1 were analyzed similarly, which are shown in Supplementary Figs. S9 (THF), S14 ([C_{12}mim][NTf_2]), and S15 ([P_{8881}][NTf_2]). The parameters obtained from the fit are listed in Supplementary Tables S5 and S6. The CT rate (k_{CT}) was estimated from the amplitude-weighted average of the time constants (τ_1 and τ_2) of the 2nd SV components ($k_{CT}^{-1} = (a_1\tau_1 + a_2\tau_2)/(a_1 + a_2)$), and the results are summarized in Table 1 together with the solvent viscosity (η).[52–56]

Figure 7 shows the results of the polar solvent ACN. We plotted the 1st, 2nd, and 3rd spectral components of the time-resolved fluorescence in Fig. 7a. For this case, we got better results by including the 3rd spectral component. The spectral components of the fluorescence are similar to those of toluene. The 1st one is a single band centered around 15,000 cm^{-1}. The 2nd and 3rd components show a positive band on the blue side of the band of the 1st component, and a negative band on the red side of each positive band. The time profiles as shown in Fig. 7b show features similar to those of toluene (Fig. 6b). The changes in the 2nd and 3rd components cause a red shift of the fluorescence with time. The 1st spectral component of the transient absorption has a broad absorption at ~18,000 cm^{-1} (550 nm) and a bleach band at ~22,000 cm^{-1} (450 nm) (Fig. 7c). The 2nd one has a negative band at ~19,000 cm^{-1} (530 nm) and a positive band at ~18,000 cm^{-1} (550 nm). The 3rd one has negative bands at ~23,000 and 17,000 cm^{-1} (430 and 590 nm) and a positive band at 16,000 cm^{-1} (620 nm). The initial variations of 2nd and 3rd components express the fast initial spectral dynamics (Fig. 7d). The time profile of each component was similarly fitted simultaneously, and the results are shown by the black curves. The results of SVD analysis for DCM, acetone, MeOH, and [C_4mim][NTf_2] are summarized in Supplementary Figs. S10 to S13 and analyzed similarly. The parameters obtained from the fit are listed in Supplementary Tables S5 and S6.

In polar solvents, several time constants for the initial dynamics were observed for fluorescence and transient absorption from SVD analysis. The fastest one <0.5 ps may be due to the solvation dynamics and coherent artifact of the laser pulses. Therefore, we concluded that τ_2 in Supplementary Tables S5 and S6 corresponds to the time constant of CT formation for the case of acetone and MeOH. For DCM, ACN, and [C_4mim][NTf_2], we calculated the amplitude-weighted average of τ_2 and τ_3 for the fluorescence time profile of the 1st SV as the CT state formation time. The rate constants (k_{CT}) thus calculated are listed in Table 1. It is to be noted here that we neglected the contribution of the spectral shift due to the solvation which may contribute the spectral dynamics. This may be included into the spectral shift and population dynamics from FC to CT states.

Now the point is how to estimate the formation rate of TICT (k_2). From theoretical calculations, the oscillator strength of the transition of TICT between the excited and ground states is quite small, and the TICT state is dark in the fluorescence spectrum. Therefore, the TICT state does not explicitly contribute to the fluorescence spectrum. In our analysis, the transient absorption spectra could be analyzed using the same time constants of the time-resolved fluorescence. If the lifetime of the TICT state is long enough, the absorption of the TICT state may have a long-time contribution to the spectrum, or the bleach recovery of the ground state may be slow in comparison with the fluorescence decay of the CT state, as indicated by Eq. (6). Supplementary Fig. S16 shows the bleach recovery transients in ACN and MeOH. In both solvents, the recovery times (120 ps for ACN and 22 ps for MeOH) were almost the same as the fluorescence decay constants. Therefore, the decay rate of the TICT is faster than the formation rate of the TICT ($k_2 < k_5$). In this

case, the apparent fluorescence decay rate (k_f) corresponds to the sum (k_B) of the TICT formation rate (k_2) and the nonreactive decay rate of the CT state (k_4). If the nonreactive decay of the CT state is assumed to similar to the value in the solvent which shows the fastest fluorescence decay without TICT formation ([C_{12}mim][NTf_2]), the TICT formation rate in each solvent can be estimated from the fluorescence decay rate constant ($k_2 = k_f - k_f$ ([C_{12}mim][NTf_2])). The time constants obtained are listed in Table 1.

The CT formation rate is not very different among the conventional solvents, while the rate in ILs is relatively slow. This is probably due to the high viscosity of the ILs. Supplementary Fig. S17 shows the plot of k_{CT} against η^{-1}. As shown in the figure, the rate is dependent on the solvent viscosity for ILs, while the dependence is not observed for the conventional liquid solvents. It is expected that the rotation of the phenyl group is hindered by the high viscosity of the solvent. Since ILs have a larger viscosity than conventional liquid solvents, the effect of the viscosity is clearly demonstrated. It is interesting to note that the photoexcitation dynamics of **1d** in ILs with long alkyl chains were similar to nonpolar solvents. Although the polarity of these ILs is high as demonstrated by solvatochromic parameters,[30] the existence of the nonpolar domain may affect the reaction dynamics of **1d**. Further, the high viscosity of these ILs hindered the further rotation of the phenyl ring.

Supplementary Fig. S18 shows the plot of k_{TICT} against $F(\varepsilon_0, n)$. The formation rate of TICT seems to increase with increasing the solvent polarity. It is to be noted that the dielectric continuum model may not be applied to the result of ILs ([C_4mim][NTf_2]), considering that the polarity scale is much larger than is expected from the dielectric constant.[28,29] If the effective dielectric constant of [C_4mim][NTf_2] is as large as that of ACN, the result in [C_4mim][NTf_2] may be closer to the correlation with conventional liquid solvents. According to the theoretical calculations, the estimated activation barrier is rather small even in toluene.[16] However, the TICT state was not detected in toluene, and the correlation shown in Supplementary Fig. S18 suggests the TICT formation is governed by the solvent polarity. The stabilization of the TICT state by the solvent polarity reduces the activation energy of the reaction. The energy profile of the CT to the TICT state should be explored in more detail theoretically.

3.5 Photoexcitation dynamics of azaphosphole with an OH group (1e)

Intramolecular proton transfer (IPT) occurs in the compound with the -OH group at the *ortho* position of the phenyl ring (**1e-OH**) to form a tautomer (**1e-NH**) as demonstrated previously.[15] The time-resolved fluorescence spectra of **1e-OH** in toluene and DCM showed dual emissions from **1e-OH** and **1e-NH** at different wavelengths indicating the existence of the excited-state IPT (ESIPT).[15] Supplementary Fig. S19a shows the time-resolved fluorescence in ACN. As shown previously, dual emissions were observed at ~22,000 and 16,000 cm^{-1} (Supplementary Fig. S19b). The former corresponds to the normal excited state (**1e-OH**), which decayed within the time-resolution of our system. The latter corresponds to the tautomer excited state (**1e-NH**), which decays with a time constant of 2.0 ps (Supplementary Fig. S19c). The decay of the tautomer was faster in the polar solvent (ACN) than in the nonpolar solvent (toluene).

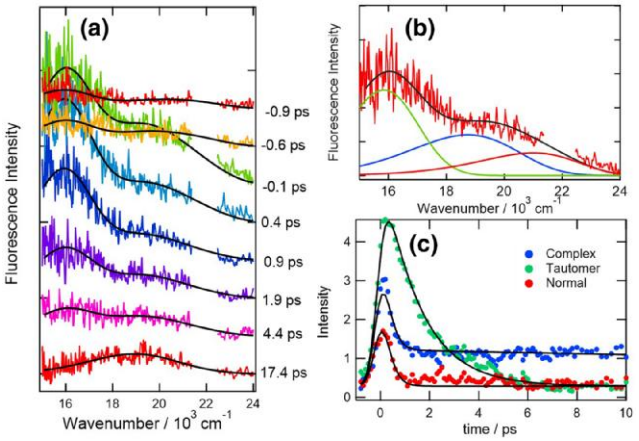

Fig. 8. a) Time-resolved fluorescence of **1e-OH** in MeOH. b) Spectral decompositions into the normal, tautomer, and complex fluorescence. c) Time profile of the band intensity of normal, tautomer, and complex.

Different spectral dynamics were observed in MeOH. Figure 8 shows time-resolved fluorescence spectra in MeOH. As observed in aprotic solvents, fluorescence bands around 22,000 and 16,000 cm^{-1} appeared as in aprotic solvents, and another band centered around 19,000 cm^{-1} appeared almost simultaneously. In order to analyze spectral dynamics, we assumed that 3 spectral components contribute to the fluorescence spectrum, and tried to decompose them by fitting with a sum of 3 log normal functions. The details of the spectra fit are described in Supplementary Section S3. The black curves in Fig. 8 are the results of the fitting, which capture the spectral features well, although there remained ambiguity on the spectral decomposition of the normal fluorescence around 22,000 cm^{-1} and the fluorescence around 19,000 cm^{-1}. Figure 8b shows the results of the spectral decomposition and their time profiles are shown in Fig. 8c. The fast decay of the band centered around 19,000 cm^{-1} may be due to the artifact of the incompleteness of the spectral decomposition, because the spectral position of the N* band is close to the band around 19,000 cm^{-1}. The decay of the band around 19,000 cm^{-1} was much slower than the tautomer decay (Supplementary Fig. S20).

Figure 9 shows the transient absorption spectra of the same system obtained at 350 nm excitation. To observe the absorption bleach around 400 nm, the excitation wavelength of 350 nm was chosen. The spectral shape was similar to that reported previously for toluene solution. Compared with toluene,[15] the spectrum shows an transient absorption band at ~580 nm, where the decay is slow. The time profiles at the selected wavelengths are shown in Figs. 9b to d. The band around 450 nm (Fig. 9b) decayed rapidly, and the decay constant was 3.0 ps, which was close to the decay constant determined by fluorescence measurement. At the longer wavelength 573 nm (Fig. 9c), we observed a longer time component (127 ps). The bleach signal was initially observed around the ground-state absorption wavelength, which was recovered by shifting its center wavelength. The spectral shift suggests that a new absorption band appeared on the blue side owing to the newly appeared species. The recovery at 410 nm was slow (Fig. 9d). The time constants obtained by fitting are summarized in Table 2 and Supplementary Table S7.

As was done previously,[15] we calculated the electronic structures using DFT for the solvent methanol (PCM).

Differently from the previous calculations, we used the functional ωB97X-D to account for the long-range interaction. Figure 10 shows the energy scheme obtained for the methanol solution. The Cartesian coordinates and computed total energies are summarized in Supplementary Table S8. As in previous calculations, the energy of **1e-NH** in the electronic excited state is lower than that of **1e-OH**, suggesting the occurrence of proton transfer in the excited state. The fluorescence wavelength of **1e-NH** is expected to be longer than that of **1e-OH**, in accordance with the interpretation of the experimental results.

In order to seek a probable origin of the new appeared fluorescence in MeOH, we assumed a cluster model of **1e-OH** with one methanol molecule. There are several possible hydrogen-bonding structures between **1e-OH** and MeOH. We found local minima where the OH proton of methanol forms hydrogen bond with the nitrogen atom of the phosphole ring, thereby prohibiting proton transfer. Figure 11 shows an energy diagram of the complex. Two different conformers with similar energies were obtained. One is the case where the methyl group of MeOH is oriented toward the oxygen side of the phosphole ring, and the other is the case where the methyl group of MeOH is oriented toward the phenyl side of the phosphole ring. In both cases, the fluorescence wavelength is slightly red-shifted to the **1e-OH** fluorescence, as shown in Fig. 11. A similar type of hydrogen-bonding complex has been reported for flavonols[57,58] and benzothiazole.[59,60] Klymchenko and Demchenko[57] have studied the solvent effects on the ESIPT of 4′-*N*,*N*-diethylamino-3-hydroxyflavone (C_2HF) including protic solvents. They found that the hydrogen bond donating property of the solvent had an additional effect on reducing the ESIPT yield, that is, hydrogen bonding from a

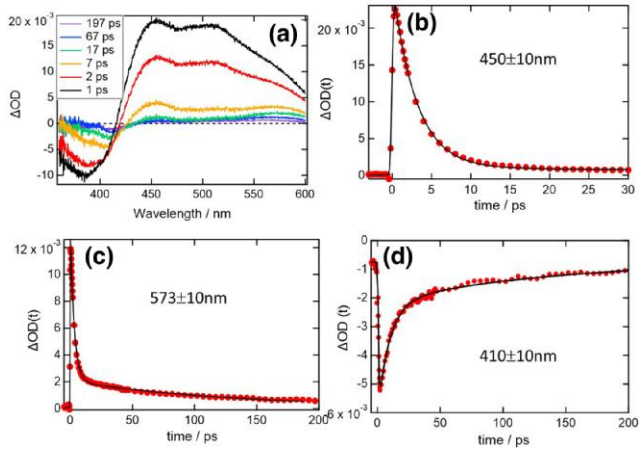

Fig. 9. a) Transient absorption spectra of **1e-OH** in MeOH excited at 350 nm. Time profiles at the selected wavelength are shown at b) 450 nm, c) 573 nm, and d) 410 nm.

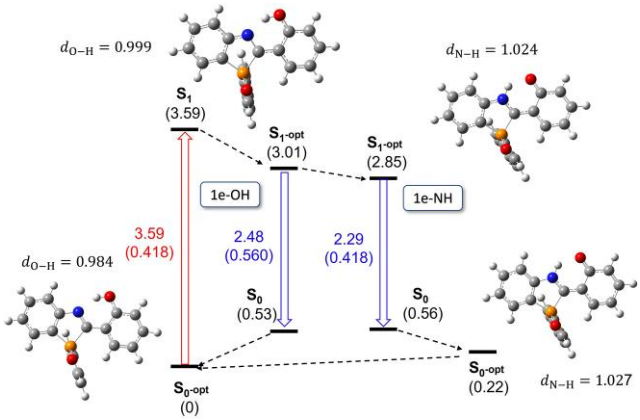

Fig. 10. Energy diagrams of the ground and excited states calculated by DFT. The relative energies (in eV) are indicated in black in parentheses. S_0-opt and S_1-opt denote the optimized S_0 and S_1 structures, respectively. Transition energies (in eV) and oscillator strengths (in parentheses) calculated by TD-DFT are indicated beside the up-arrow (absorption, in red) or the down-arrow (fluorescence, inblue). The OH distance (d_{O-H}) of **1e-OH** and the N-H distance (d_{N-H}) of **1e-NH** are indicated (in Å).

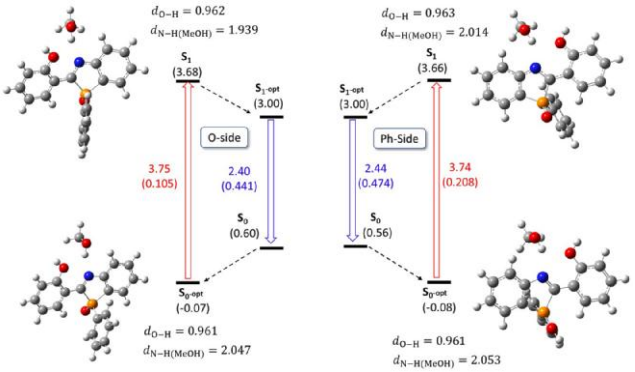

Fig. 11. Energy diagrams of the ground and excited states of the complexes calculated by DFT. The relative energies (in eV) are indicated in black in parentheses. S_0-opt and S_1-opt denote the optimized S_0 and S_1 structures, respectively. The energy standard is taken as the state where a methanol molecule and 1e-OH are separated infinitely. Transition energies (in eV) and oscillator strengths (in parentheses) calculated by TD-DFT are indicated beside the up-arrow (absorption, in red) or the down-arrow (fluorescence, in blue). The OH distance (d_{O-H}) of **1e-OH** and the NH distance between the nitrogen atom of **1e-OH** and the hydrogen atom of -OH of MeOH ($d_{N-H(MeOH)}$) are shown (in Å). .

Table 2. Summary of the spectroscopic data and time constants of decay obtained from the analysis of the fluorescence spectra for **1e-OH.**

			τ_f/ps		
Solvent	λ_{abs}/nm	Φ_f	T*	N*	C*
Toluene	351, 395[a]	<0.01[a]	3.8 ± 0.2[a]	<0.2[a]	–[b]
DCM	350, 392[a]	<0.01[a]	3.8 ± 0.2[a]	<0.2[a]	–[b]
ACN	349, 394	–[c]	2.0 ± 0.2	<0.2	–[b]
MeOH	345, 389	–[c]	1.5 ± 0.1	<0.2	<0.2, 41 ± 9 (0.68)[d], 127(f) (0.32)[d]

[a]Nakagomi et al.[15]
[b]Not detected.
[c]Not determined.
[d]Values in the parenthesis show the relative contribution of the second and the third time constants.

protic solvent to the proton acceptor site of C_2HF prohibits ESIPT. A similar phenomenon may be observed in this case. Therefore, we consider that the hydrogen-bonding complex contributes to the long-time fluorescence. Experimentally, however, the ground state absorption was not so different from those in other aprotic solvents (Supplementary Fig. S21). The complex between methanol and **1e-OH** is not as strong as expected from the cluster model.

4. Conclusion

In summary, we have revealed the photoexcitation dynamics of ABPO by ultrafast spectroscopy. The fluorescence lifetimes of ABPO were generally shorter than those of isoelectronic benzo[*b*]phosphole oxides. The high electron-accepting ability of the azaphosphole ring was also reflected in the solvatochromic behavior of the *para*-NPh_2 derivative (**1d**). The fluorescence dynamics of **1d** were investigated in detail based on theoretical predictions. The spectral dynamics from the FC state to the CT state were identified in nonpolar and polar solvents. Furthermore, in polar solvents, the existence of the TICT state predicted by theoretical calculations was revealed. The CT process was controlled by the solvent viscosity, as evidenced by the results for the ILs.

The *ortho*-hydroxyphenyl derivative underwent ESIPT in the solution to emit dual fluorescence. However, in methanol, another fluorescence species appeared in addition to the excited states of **1e-OH** and **1e-NH**. DFT calculations suggested that the hydrogen-bonded complex of **1e-OH** with methanol might be the origin of the new fluorescence species.

As demonstrated by present work, replacement of the β-methine unit of the phosphole ring with a nitrogen atom did not bring about high-fluorescent compounds, although various unique photodynamics were observed by the variation of aryl group at the 2-position. Further researches on the variations of phosphole are expected to bring about unique photochemistry never reported.

Supplementary data

Supplementary material is available at *Bulletin of the Chemical Society of Japan* online.

Funding

This work was supported by Grants-in-Aid for Scientific Research from Japan Society for the Promotion of Science (JSPS KAKENHI; grant number 22H02061 to Y.M., 21K04980 to H.N., and 22H02040 to Y.K.).

Conflict of interest statement. None declared.

Data availability

Data will be available on request.

References

1. D. Joly, P. A. Bouit, M. Hissler, *J. Mater. Chem. C* **2016**, *4*, 3686. https://doi.org/10.1039/C6TC00590J
2. Y.-H. Cheng, H.-L. Wong, E. Y.-H. Hong, S.-L. Lai, M.-Y. Chan, V. W.-W. Yam, *ACS Appl. Energy Mater.* **2020**, *3*, 3059. https://doi.org/10.1021/acsaem.0c00189
3. C. Wang, A. Fukazawa, M. Taki, Y. Sato, T. Higashiyama, S. Yamaguchi, *Angew. Chem. Int. Ed.* **2015**, *54*, 15213. https://doi.org/10.1002/anie.201507939
4. C. Wang, M. Taki, Y. Sato, A. Fukazawa, T. Higashiyama, S. Yamaguchi, *J. Am. Chem. Soc.* **2017**, *139*, 10374. https://doi.org/10.1021/jacs.7b04418
5. C. Wang, M. Taki, K. Kajiwara, J. Wang, S. Yamaguchi, *ACS Mater. Lett.* **2020**, *2*, 705. https://doi.org/10.1021/acsmaterialslett.0c00147
6. T. Ichikawa, M. Morimoto, H. Sotome, S. Ito, H. Miyasaka, M. Irie, *Dyes Pigm.* **2016**, *126*, 186. https://doi.org/10.1016/j.dyepig.2015.11.023
7. N. M. Wu, M. Ng, V. W. Yam, *Nat. Commun.* **2022**, *13*, 33. https://doi.org/10.1038/s41467-021-27711-9
8. H. Tsuji, K. Sato, Y. Sato, E. Nakamura, *Chem. Asian J.* **2010**, *5*, 1294. https://doi.org/10.1002/asia.201000093
9. Y. Matano, A. Saito, T. Fukushima, Y. Tokudome, F. Suzuki, D. Sakamaki, H. Kaji, A. Ito, K. Tanaka, H. Imahori, *Angew. Chem. Int. Ed.* **2011**, *50*, 8016. https://doi.org/10.1002/anie.201102782
10. Y. Matano, A. Saito, Y. Suzuki, T. Miyajima, S. Akiyama, S. Otsubo, E. Nakamoto, S. Aramaki, H. Imahori, *Chem. Asian J.* **2012**, *7*, 2305. https://doi.org/10.1002/asia.201200492
11. Y. Matano, *Chem. Rec.* **2015**, *15*, 636. https://doi.org/10.1002/tcr.201402101
12. A. Saito, T. Miyajima, M. Nakashima, T. Fukushima, H. Kaji, Y. Matano, H. Imahori, *Chem. Eur. J.* **2009**, *15*, 10000. https://doi.org/10.1002/chem.200901378
13. Y. Hayashi, Y. Matano, K. Suda, Y. Kimura, Y. Nakao, H. Imahori, *Chem. Eur. J.* **2012**, *18*, 15972. https://doi.org/10.1002/chem.201203047
14. Y. Matano, Y. Motegi, S. Kawatsu, Y. Kimura, *J. Org. Chem.* **2015**, *80*, 5944. https://doi.org/10.1021/acs.joc.5b00541
15. H. Nakagomi, N. Murayama, R. Takegami, K. Fujii, R. Kitakado, Y. Kimura, M. Minoura, H. Nakano, Y. Matano, *Chem. Eur. J.* **2024**, *30*, e202400807. https://doi.org/10.1002/chem.202400807
16. K. Sugiyama, Y. Kimura, Y. Matano, H. Sato, M. Higashi, *J. Phys. Chem. B* **2025**, *129*, 2701. https://doi.org/10.1021/acs.jpcb.4c05872
17. K. Das, N. Sarkar, A. K. Ghosh, D. Majumdar, D. N. Nath, K. Bhattacharyya, *J. Phys. Chem.* **1994**, *98*, 9126. https://doi.org/10.1021/j100088a006
18. C. Chudoba, S. Lutgen, T. Jentzsch, E. Riedle, M. Woerner, T. Elsaesser, *Chem. Phys. Lett.* **1995**, *240*, 35. https://doi.org/10.1016/0009-2614(95)00506-Y
19. H. Zhang, P. van der Meulen, M. Glasbeek, *Chem. Phys. Lett.* **1996**, *253*, 97. https://doi.org/10.1016/0009-2614(96)00213-8
20. S. Ameer-Beg, S. M. Ormson, R. G. Brown, P. Matousek, M. Towrie, E. T. J. Nibbering, P. Foggi, F. V. R. Neuwahl, *J. Phys. Chem. A* **2001**, *105*, 3709. https://doi.org/10.1021/jp0031101
21. P. Purkayastha, N. Chattopadhyay, *J. Mol. Struct.* **2002**, *604*, 87. https://doi.org/10.1016/S0022-2860(01)00647-0
22. J. Ouyang, C. Ouyang, Y. Fujii, Y. Nakano, T. Shoda, T. Nagano, *J. Heterocycl. Chem.* **2009**, *41*, 359. https://doi.org/10.1002/jhet.5570410309
23. R. Wang, D. Liu, K. Xu, J. Li, *J. Photochem. Photobiol. A Chem.* **2009**, *205*, 61. https://doi.org/10.1016/j.jphotochem.2009.03.025
24. S. K. Behera, G. Sadhuragiri, P. Elumalai, M. Sathiyendiran, G. Krishnamoorthy, *RSC Adv.* **2016**, *6*, 59708. https://doi.org/10.1039/C6RA11780E
25. V. R. Mishra, C. W. Ghanavatkar, N. Sekar, *ChemistrySelect* **2020**, *5*, 2103. https://doi.org/10.1002/slct.201904558
26. K. Nishikawa, Y. Ouchi, T. Ito, H. Ohno, M. Watanabe, *Science of Ionic Liquid*. Maruzen, Tokyo, **2012**.
27. P. Wasserscheid, T. Welton, *Ionic Liquids in Synthesis*, 2nd ed. Wiley-VCH, Weinheim, **2008**.

28. C. Daguenet, P. J. Dyson, I. Krossing, A. Oleinikova, J. Slattery, C. Wakai, H. Weingartner, *J. Phys. Chem. B* **2006**, *110*, 12682. https://doi.org/10.1021/jp0604903
29. L. Crowhurst, P. R. Mawdsley, J. M. Perez-Arlandis, P. A. Salter, T. Welton, *Phys. Chem. Chem. Phys.* **2003**, *5*, 2790. https://doi.org/10.1039/B303095D
30. Y. Kimura, T. Fukui, S. Okazoe, H. Miyabayashi, T. Endo, *J. Mol. Liq.* **2019**, *289*, 111128. https://doi.org/10.1016/j.molliq.2019.111128
31. M. G. Del Pópolo, G. A. Voth, *J. Phys. Chem. B* **2004**, *108*, 1744. https://doi.org/10.1021/jp0364699
32. J. N. Canongia Lopes, A. A. Pádua, *J. Phys. Chem. B* **2006**, *110*, 3330. https://doi.org/10.1021/jp056006y
33. A. Triolo, O. Russina, H. J. Bleif, E. Di Cola, *J. Phys. Chem. B* **2007**, *111*, 4641. https://doi.org/10.1021/jp067705t
34. M. Kofu, M. Nagao, T. Ueki, Y. Kitazawa, Y. Nakamura, S. Sawamura, M. Watanabe, O. Yamamuro, *J. Phys. Chem. B* **2013**, *117*, 2773. https://doi.org/10.1021/jp312608r
35. E. W. Castner Jr, C. J. Margulis, M. Maroncelli, J. F. Wishart, *Ann. Rev. Phys. Chem.* **2011**, *62*, 85. https://doi.org/10.1146/annurev-physchem-032210-103421
36. R. Hayes, G. G. Warr, R. Atkin, *Chem. Rev.* **2015**, *115*, 6357. https://doi.org/10.1021/cr500411q
37. Y. L. Wang, B. Li, S. Sarman, F. Mocci, Z. Y. Lu, J. Yuan, A. Laaksonen, M. D. Fayer, *Chem. Rev.* **2020**, *120*, 5798. https://doi.org/10.1021/acs.chemrev.9b00693
38. Y. Kimura, *Pure Appl. Chem.* **2020**, *92*, 1695. https://doi.org/10.1515/pac-2019-1116
39. K. Fujii, Y. Kimura, *Chem. Rec.* **2023**, *23*, e202200242. https://doi.org/10.1002/tcr.202200242
40. H. Miyabayashi, K. Fujii, T. Watanabe, Y. Matano, T. Endo, Y. Kimura, *J. Phys. Chem. B* **2021**, *125*, 5373. https://doi.org/10.1021/acs.jpcb.1c02360
41. S. Nomura, K. Fujii, H. Sugihara, T. Endo, Y. Kimura, *J. Phys. Chem. B* **2024**, *128*, 6549. https://doi.org/10.1021/acs.jpcb.4c02573
42. R. Krishnan, J. S. Binkley, R. Seeger, J. A. Pople, *J. Chem. Phys.* **1980**, *72*, 650. https://doi.org/10.1063/1.438955
43. J. D. Chai, M. Head-Gordon, *Phys. Chem. Chem. Phys.* **2008**, *10*, 6615. https://doi.org/10.1039/b810189b
44. E. Cancès, B. Mennucci, J. Tomasi, *J. Chem. Phys.* **1997**, *107*, 3032. https://doi.org/10.1063/1.474659
45. Gaussian 16, *Revision C.01*, Gaussian, Inc., Wallingford CT, **2019**.
46. E. Z. Lippert, *Naturforsch* **1955**, *10a*, 541. https://doi.org/10.1515/zna-1955-0707
47. E. G. McRae, *J. Phys. Chem.* **1957**, *61*, 562. https://doi.org/10.1021/j150551a012
48. N. Mataga, Y. Kaifu, M. Koizumi, *Bull. Chem. Soc. Jpn.* **1956**, *29*, 465. https://doi.org/10.1246/bcsj.29.465
49. M. L. Horng, J. A. Gardecki, A. Papazyan, M. Maroncelli, *J. Phys. Chem.* **1995**, *99*, 17311. https://doi.org/10.1021/j100048a004
50. L. Reynolds, J. A. Gardecki, S. J. V. Frankl, M. L. Horng, M. Maroncelli, *J. Phys. Chem.* **1996**, *100*, 10337. https://doi.org/10.1021/jp953110e
51. N. Saleh, J. F. Kauffman, *J. Phys. Chem. A* **2004**, *108*, 7139. https://doi.org/10.1021/jp048279j
52. The Chemical Society of Japan. *Kagaku Binran*, 5th ed. Maruzen, Tokyo, **2004**.
53. M. Tariq, P. J. Carvalho, J. A. P. Coutinho, I. M. Marrucho, J. N. C. Lopes, L. P. N. Rebelo, *Flu. Phase Equil.* **2011**, *301*, 22. https://doi.org/10.1016/j.fluid.2010.10.018
54. R. C. Reid, J. M. Prausnitz, B. E. Poling, *The Properties of Gases and Liquids*, McGraw-Hill Book, Co., Singapore, **1988**.
55. P. Droliya, A. K. Nain, *J. Mol. Liq.* **2017**, *241*, 549. https://doi.org/10.1016/j.molliq.2017.06.021
56. K. Fujii, T. Yagi, H. Nakano, H. Sato, Y. Kimura, *J. Chem. Phys.* **2021**, *154*, 154504. https://doi.org/10.1063/5.0047663
57. A. S. Klymchenko, A. P. Demchenko, *Phys. Chem. Chem. Phys.* **2003**, *5*, 461. https://doi.org/10.1039/b210352d
58. C. A. Kenfack, A. S. Klymchenko, G. Duportail, A. Burger, Y. Mély, *Phys. Chem. Chem. Phys.* **2012**, *14*, 8910. https://doi.org/10.1039/c2cp40869d
59. Q. Chen, C. Jia, Y. Zhang, W. Du, Y. Wang, Y. Huang, Q. Yang, Q. Zhang, *J. Mater. Chem. B* **2017**, *5*, 7736. https://doi.org/10.1039/C7TB02076G
60. K. Naka, H. Sato, M. Higashi, *Phys. Chem. Chem. Phys.* **2021**, *23*, 20080. https://doi.org/10.1039/D0CP06604D